NANO LETTERS

Letter

Cite This: Nano Lett. 2019, 19, 3143−3150

pubs.acs.org/NanoLett

Optomechanical Measurement of Thermal Transport in Two-Dimensional $MoSe_2$ Lattices

Nicolas Morell,[†] Slaven Tepsic,[†] Antoine Reserbat-Plantey,[†] Andrea Cepellotti,[‡,§] Marco Manca,[∥] Itai Epstein,[†] Andreas Isacsson,[⊥] Xavier Marie,[∥] Francesco Mauri,[#] and Adrian Bachtold*,[†]

[†]ICFO - Institut de Ciencies Fotoniques, The Barcelona Institute of Science and Technology, 08860 Castelldefels, Barcelona, Spain

[‡]Department of Physics, University of California at Berkeley, Berkeley, California 94720, United States

[§]Materials Sciences Division, Lawrence Berkeley National Laboratory, Berkeley, California 94720, United States

[∥]Université de Toulouse, INSA-CNRS-UPS, LPCNO, 135 Avenue Rangueil, 31077 Toulouse, France

[⊥]Department of Physics, Chalmers University of Technology, S-41296 Göteborg, Sweden

[#]Dipartimento di Fisica, Università di Roma La Sapienza, Piazzale Aldo Moro 5, I-00185 Rome, Italy

Supporting Information

ABSTRACT: Nanomechanical resonators have emerged as sensors with exceptional sensitivities. These sensing capabilities open new possibilities in the studies of the thermodynamic properties in condensed matter. Here, we use mechanical sensing as a novel approach to measure the thermal properties of low-dimensional materials. We measure the temperature dependence of both the thermal conductivity and the specific heat capacity of a transition metal dichalcogenide monolayer down to cryogenic temperature, something that has not been achieved thus far with a single nanoscale object. These measurements show how heat is transported by phonons in two-dimensional systems. Both the thermal conductivity and the specific heat capacity measurements are consistent with predictions based on first-principles.

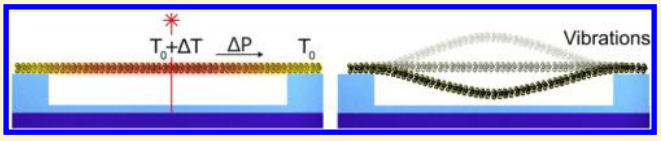

KEYWORDS: *Optomechanical resonator, thermal transport, specific heat, transition metal dichalcogenide, $MoSe_2$, monolayer, NEMS*

Mechanical resonators based on suspended nanoscale objects, such as monolayer semiconductors,[1−4] graphene,[5−16] nanotubes,[17−28] and semiconducting nanowires,[29−36] have attracted considerable interest. Because of their small mass, such resonators become fantastic sensors of external forces and the adsorption of mass.[21,23,27,37] The sensing capabilities of nano- and microresonators have been used with great success in recent advances of various fields. These include nanomagnetism,[38,39] surface imaging,[35,36] surface science,[40,41] light-matter interaction,[32] persistent currents in normal metal rings,[42] and engineered electron−phonon coupling.[25] In this work, we show how optomechanical systems can be used to study heat transport in individual low-dimensional materials.

Heat transport at the nanoscale is of major fundamental interest for a broad range of research fields, such as nanophononics,[43−45] spintronics,[46] quantum electron devices,[47,48] and quantum thermodynamics.[49] Heat can be controlled and measured with good accuracy in devices microfabricated from bulk material. By contrast, heat transport in devices based on low-dimensional materials cooled at low temperature is still at its infancy. Measuring their thermal conductance at cryogenic temperature is a challenging task. It requires the fabrication of sophisticated devices, which incorporate local heaters and thermometers, and a careful calibration of the latter.[50,51] The difficulty of fabricating reliable devices has hindered progress in the field for many years.

Lattice vibrations are the main carriers of heat in a large variety of low-dimensional materials, including carbon nanotubes,[51,52] graphene,[53] and semiconductor monolayers.[54] Heat transport has been intensively studied at room temperature and above using Raman measurements[55−62] and scanning probe microscopy.[63,64] Heat transport enters into interesting regimes at low temperature, such as the dissipationless transport through low-dimensional materials in the ballistic regime[50,51,65] and the phonon hydrodynamic regime predicted in monolayers.[66,67] The interpretation of heat transport measurements can be difficult, since the thermal conductance depends on various quantities that have not been measured independently thus far. These include the heat capacity and the phononic mean-free path. Recently, new methods have been reported to measure the electron contribution of the thermal conductivity of graphene down to low temperature.[68,69]

Heat transport measurements in low-dimensional materials have mainly consisted in probing the thermal conductance K, that is, how well the system conducts heat. In optomechanics, it is possible to measure how quickly the mechanical resonator conducts heat.[70−72] The characteristic time τ for the heat to

Received: February 7, 2019
Revised: March 28, 2019
Published: April 2, 2019

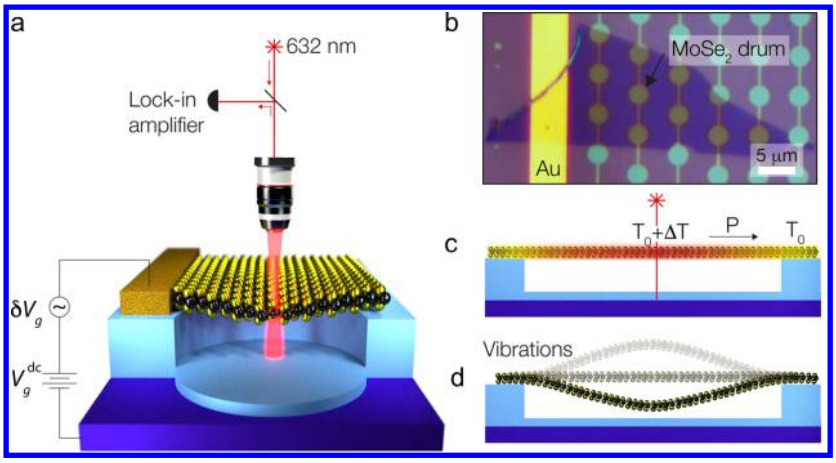

Figure 1. Optomechanical device structure and working principle used to measure thermal transport. (a) Schematic of the optomechanical device. The mechanical vibrations are driven capacitively and detected by optical interferometry.[3] The $MoSe_2$ monolayer is a mobile absorber in an optical standing wave produced by a 632 nm probe laser. The modulated laser reflection intensity is measured with an avalanche photodetector feeding a lock-in amplifier. (b) Optical microscopy image of a typical device. (c) Heat transport induced by the absorption of the laser power. A temperature difference ΔT is created from the heat flow. (d) Detection of the laser-induced temperature rise ΔT using the fundamental mechanical mode of the optomechanical resonator.

travel out of the resonator introduces a retarded force acting on the mechanical resonator.[73,74]

Here, we combine two methods to measure K and τ in a optomechanical resonator based on a vibrating $MoSe_2$ monolayer. This allows us to unravel the thermal properties of low-dimensional materials down to cryogenic temperature and with a device that is simple to fabricate. Our measurements indicate that the phonon transport is diffusive above ~100 K, while the majority of phonon carriers are ballistic over the size of the device at low temperature. The temperature dependence of the specific heat capacity approaches a quadratic dependence, the signature of two-dimensional lattices. Both the thermal conductance and the specific heat capacity measurements can be described by predictions based on first-principles.

The mechanical resonator consists of a $MoSe_2$ monolayer drum (Figure 1a−d). The drum is fabricated with the dry transfer of $MoSe_2$ monolayers using a polydimethylsiloxane (PDMS) stamp[75] over a highly doped Si substrate with prestructured holes. $MoSe_2$ monolayers are obtained from mechanical exfoliation of crystals purchased from 2D semiconductors. The device is measured in a cryostat whose temperature can be set between 3 and 300 K. Photoluminescence spectra at 3 K feature narrow peaks associated with two-dimensional excitons and trions with a wavelength at ~762 and ~748 nm, respectively (Section 1 of Supporting Information), in agreement with previous reports.[76,77] Photoluminescence maps are homogeneous.[3] These measurements confirm that the drums are made from $MoSe_2$ monolayers. The metal electrode attached to the $MoSe_2$ flake is used to apply an electrostatic force on the drum (Figure 1a,b); it has no effect on the thermal transport.

Mechanical vibrations are detected by optical interferometry.[3,74] A continuous wave laser impinges on the center of the $MoSe_2$ membrane, and the reflected laser light intensity is modulated by an amount proportional to displacement of the resonator. The laser forms a standing wave pattern in the direction perpendicular to the Si substrate, such that the displacement of the monolayer modifies its optical absorption. The laser spot has a measured radius of about 350 nm. Measuring the mechanical resonator with the laser beam modifies the dynamics of the mechanical vibrations by a small amount; increasing the laser power modifies the resonance frequency and the resonance line width (Figure 2). This backaction has two components, the static and the dynamical backaction. The former allows us to quantify K, and the latter τ.

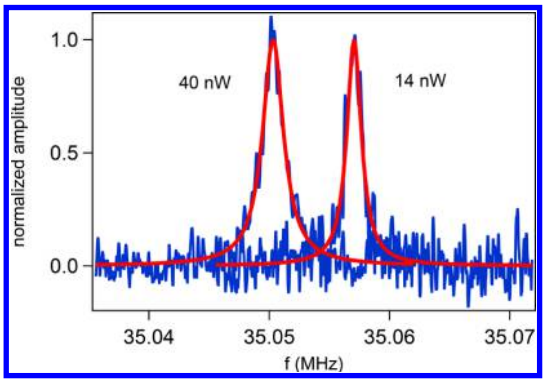

Figure 2. Backaction of the laser on mechanical vibrations. Response of the displacement amplitude of the mechanical mode as a function of the frequency of the driving force for two different absorbed laser powers. The temperature is set at 3 K and the gate voltage at 4 V. The red lines correspond to Lorentzian fits.

We measure the thermal conductance in a way similar to the well-established method based on Raman measurements employed at room temperature.[55,56] The static backaction of the laser beam is a simple absorption heating effect, which results in a temperature gradient ΔT between the center of the membrane and its circular clamp (Figure 1c). The heat flow is given by the power P absorbed in the membrane (Section 2 of Supporting Information). In a Raman measurement, ΔT is quantified by the frequency shift of Raman-active peaks. In our case, ΔT is measured by the frequency shift Δf_T of the fundamental mechanical mode (Figure 1d). As a result, the equivalent thermal conductance is $K = P/\Delta T$. Mechanical $MoSe_2$ drums with their high quality factor[3] are extremely good temperature sensors, allowing us to measure the linear

DOI: 10.1021/acs.nanolett.9b00560
Nano Lett. 2019, 19, 3143−3150

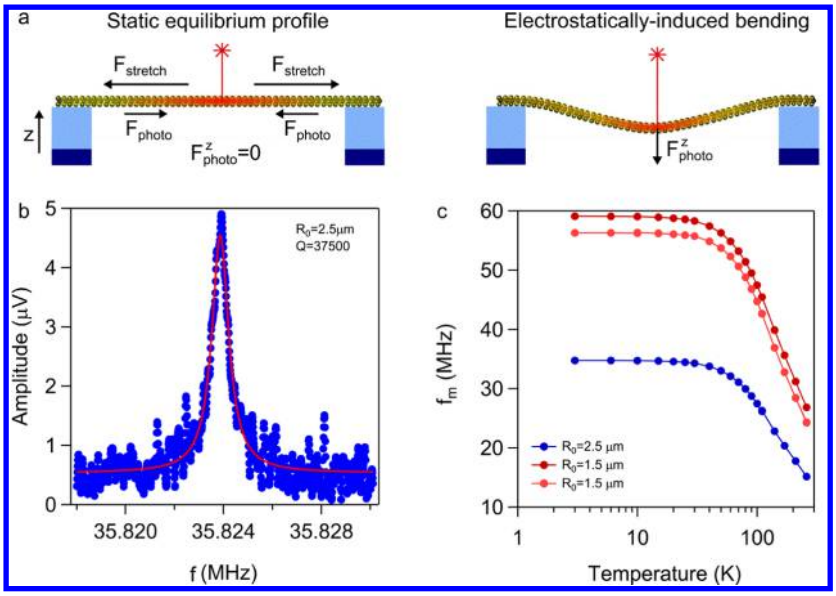

Figure 3. $MoSe_2$ drum under mechanical tension. (a) Static profile of the drum controlled with an electrostatic force by applying the tension V_g^{dc} on the backgate (Figure 1a). In the straight configuration, the measured frequency shift is solely related to static backaction, which allows us to quantify the thermal conductance. The drum is stretched by the force F_{strech} from the circular clamp. The force F_{photo} produced by the laser beam reduces the stretching. In the bending configuration, the frequency shift also depends on dynamical backaction, because $\partial_z F^z_{photo}$ is finite. This allows us to quantify the time τ for the heat to travel out from the drum. The amplitude of the mechanical vibrations (<1 nm) is smaller than the static displacement ($\lesssim$10 nm) in the bending configuration. (b) Response of the displacement amplitude of the mechanical mode as a function of the frequency of the driving force at 3 K. (c) Resonance frequency of the mechanical mode as a function of temperature for three different devices when the drum is in the straight configuration.

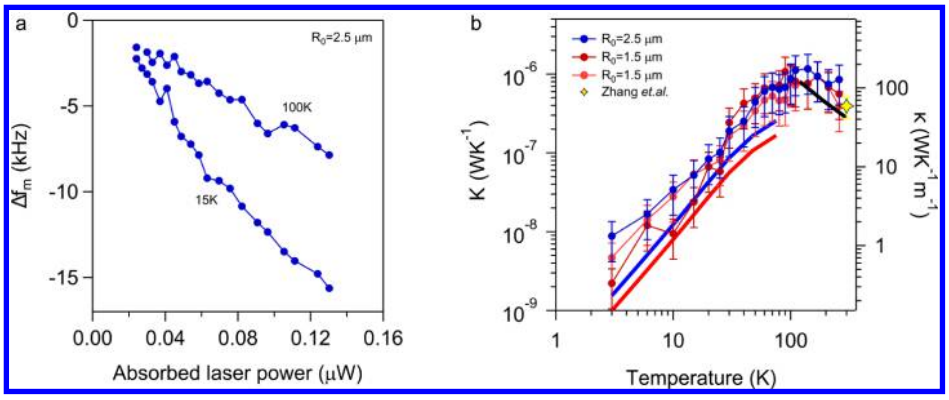

Figure 4. Thermal conductance of $MoSe_2$ monolayers. (a) Shift of the resonance frequency Δf_m as a function of absorbed laser power P when the drum is in the straight configuration. (b) Thermal conductance $K = P/\Delta T$ as a function of temperature. The right axis shows the conductivity in the diffusive regime, which is obtained using eq 4 with η = 0.61. The yellow star symbol at 300 K corresponds to the thermal conductivity measured with the Raman method;[60] we are not aware of another measurement of the thermal conductivity of $MoSe_2$ monolayers. The black line shows the conductivity in the diffusive regime for an infinitely large monolayer computed by solving the Boltzmann transport equation as in ref 84. The red and the blue line corresponds to the conductance in the ballistic regime computed from first-principles for the 1.5 and the 2.5 μm radius drum, respectively, using eq 5 with α = 2.1 and α = 3.2.

thermal conductance down to 3 K. This is a significant improvement compared to Raman measurements, which are typically operated at 300 K or above, because the detection of the frequency shift of Raman-active peaks requires comparatively large P.

We measure τ from the effect of the dynamical backaction on the electrostically driven vibrations. Absorption heating from the laser beam expands the $MoSe_2$ crystal,[3] which is equivalent to a force acting on the membrane. The crystal expansion responds to a change in the absorbed laser power with delay, that is, the time τ for the membrane to heat up or to cool down. The absorbed laser power oscillates in time because of the oscillating motion of the membrane in the laser interference pattern used to detect the vibrations. Overall, the photothermal force oscillates with a finite phase shift compared to the motion of the membrane. The in-phase photothermal force modifies the resonance frequency by Δf_B and the out-of-phase photothermal force modifies the resonance line width by $\Delta\Gamma_B$ as

$$\Delta f_B = -\frac{1}{2} f_m \frac{\partial_z F^z_{photo}}{k} \frac{1}{1 + (2\pi f_m \tau)^2} \tag{1}$$

$$\Delta\Gamma_B = f_m \frac{\partial_z F^z_{photo}}{k} \frac{2\pi f_m \tau}{1 + (2\pi f_m \tau)^2} \tag{2}$$

DOI: 10.1021/acs.nanolett.9b00560
Nano Lett. 2019, 19, 3143−3150

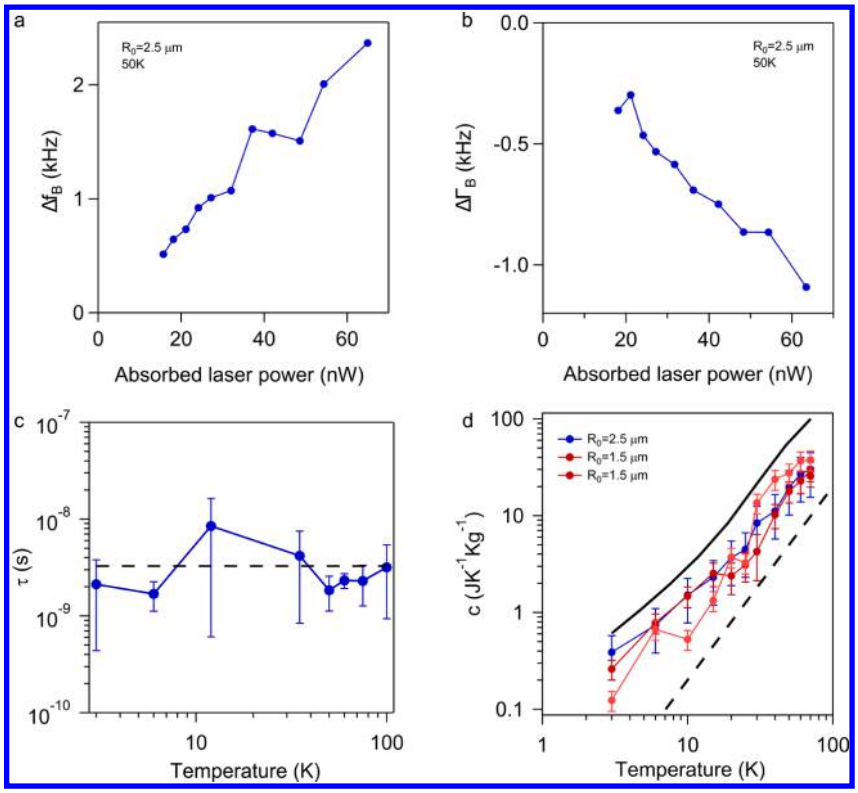

Figure 5. Time for the heat to travel out of the drum and specific heat capacity of $MoSe_2$ monolayers. (a,b) Shifts of the resonance frequency Δf_B and the mechanical bandwidth $\Delta\Gamma_B$ as a function of absorbed laser power P. We obtain Δf_B and $\Delta\Gamma_B$ by subtracting the frequency shift and the bandwidth shift measured in the bending configuration from that measured in the straight configuration. (c) Time for the heat to travel out of the drum as a function of temperature. The large error bars at 12 and 35 K are due to the drift of the resonance frequency caused by the automatized heating and cooling switches in our cryofree cryostat. The dashed black line corresponds to the averaged τ. (d) Specific heat capacity as a function of temperature. We convert $C = \langle\tau\rangle K$ into c using eq 3 with $\beta = 0.86$. The black dashed line corresponds to the T^2 dependence. The black continuous line corresponds to the specific heat capacity computed from first-principles. Since the displacement sensitivity of the 1.5 μm radius drums was not good enough to measure τ, we estimate $\langle\tau\rangle$ from the value measured with the 2.5 μm radius drum and the radius ratio. The error bars come from the uncertainty in $\langle\tau\rangle$ and K.

Here, f_m is the resonance frequency of the mechanical mode, k is its spring constant, z is the coordinate in the direction perpendicular to the membrane, and $\partial_z F^{\alpha}_{\text{photo}}$ is the derivative of the z-component of the photothermal force with respect to z. We infer τ from Δf_B and $\Delta\Gamma_B$ for a fixed laser power using $\tau = -\Delta\Gamma_B/4\pi f_m \Delta f_B$.

The key to quantify Δf_T and Δf_B is to deform the static profile of the drum with an electrostatic force (Figure 3a). The drum is straight when it is not subject to a sizable electrostatic force. This is because the drum is mechanically stretched by the circular clamp, as shown by the strong temperature dependence of f_m (Figures 3b,c); the tensile strain in the membrane is quantified by the measured dependence of f_m on the electrostatic force (Section 3 of Supporting Information).[3] The absorbed laser power generates a photothermal force F_{photo} that reduces the stretching force. When the drum is straight, the photothermal force is perpendicular to the motion of the vibrations so that $\Delta f_B = 0$ (eq 1); in this straight configuration, we only measure Δf_T associated with the thermal conductance. When the drum is bent, the photothermal force modifies both Δf_T and Δf_B. We obtain Δf_B by subtracting the frequency shifts measured in the bending and the straight configurations (Section 4 of Supporting Information). We go from a straight configuration to a bending configuration by applying a voltage V_g^{dc} onto the gate electrode.

Figure 4a,b shows the temperature dependence of the equivalent thermal conductance. The conductance is obtained from the slope $\Delta f_m/\Delta P$ in Figure 4a using the calibration slope $\Delta f_m/\Delta T$ in Figure 3c. The conductance is measured in the linear regime, because the applied P is low. The largest ΔT remains below 1 K. The estimation of the absorbed laser power is detailed in Section 2 of Supporting Information; we use 5.7% for the absorption coefficient of $MoSe_2$ monolayers.[60] We also show that the absorption coefficient is independent of temperature and gate voltage at the laser wavelength $\lambda = 632$ nm. In order to ensure that the resonance frequency and the resonance line width Γ_m depend linearly on the laser power, we estimate $\Delta f_m/\Delta P$ and $\Delta\Gamma_m/\Delta P$ for absorbed laser powers below 35 nW when the temperature is below 40 K and 60 nW otherwise. We emphasize that the temperature profile over the surface of the drum in the measurement of $\Delta f_m/\Delta P$ differs from that of $\Delta f_m/\Delta T$. This results in a prefactor in the conversion from the equivalent thermal conductance K into the thermal conductivity of the monolayer, as described below.

The temperature dependence of the thermal conductance suggests diffusive transport at high temperature (Figure 4b). Upon increasing temperature above ~100 K, the conductance decreases, which is attributed to the reduction of the mean-free path due to phonon−phonon scattering.[78] Below ~100 K, the conductance gets larger when increasing temperature. This indicates that phonon−phonon scattering is no more relevant,

DOI: 10.1021/acs.nanolett.9b00560
Nano Lett. 2019, 19, 3143−3150

so that the mean-free path could be limited by, for example, the device size or the grain boundaries of the crystal. The error bars of the thermal conductance in Figure 4b come from the uncertainty in the absorption coefficient A of the monolayer (Section 2 of Supporting Information). Because we cannot measure the absorption coefficient, we choose a large uncertainty, that is, $A = 0.057 \pm 0.03$. Figure 4b shows that this affects the measured temperature dependence of the thermal conductance only weakly.

We measure τ by comparing the resonance frequency and the resonance line width measured with the resonator in the straight configuration ($V_g^{dc} = 0$ V) and in the bending configuration ($V_g^{dc} = 4$ V) (Section 4 of Supporting Information). Here $V_g^{dc} = 4$ V is the largest voltage that we apply, because a larger voltage may collapse the drum onto the bottom of the trench. The associated strain is less than 1% (Section 3 of Supporting Information). Such a small strain is expected to have no sizable effect on the thermal transport properties.[79]

Figures 5a−c show that τ remains constant when varying temperature within the error bars of the measurements. We cannot measure τ above 100 K, because the reduced quality-factor prevents us from resolving Δf_B. Using the averaged phonon velocity $v \simeq 1300$ m/s computed by first-principles (Section 5 of Supporting Information), the average time $\langle\tau\rangle = 3.3 \pm 2.1$ ns results in a mean-free path of about 4.3 ± 2.7 μm, which is consistent with the 2.5 μm radius of the drum. This suggests that the majority of the phonon carriers are ballistic over the size of the drum.

These measurements allow us to directly quantify the equivalent heat capacity of an individual $MoSe_2$ monolayer using $C = \langle\tau\rangle K$. Figure 5d shows that the temperature dependence of the heat capacity approaches a T^2 dependence. This is consistent with the T^d dependence expected for two-dimensional systems in its simplest form, where $d = 2$ is the dimensionality. Previous measurements of the phononic heat capacity of nanomaterials were carried out by packing them in macroscopic ensembles, such as films of nanotube ropes[80] and powders of $MoSe_2$ multilayered crystals.[81] Such ensemble measurements suffer from the coupling between nanosystems, which modifies the heat capacity at low temperature.

The temperature profile along the heat flow has to be considered when evaluating the specific heat capacity c and the thermal conductivity κ of $MoSe_2$ monolayers (Figures 4b and 5d). The temperature is nonuniform over the surface of the drum when measuring the slope $\Delta f_m/\Delta P$, while it is uniform during the measurement of the calibration slope $\Delta f_m/\Delta T$. These different temperature profiles add a geometrical constant in the conversion from C and K into c and κ. In the ballistic regime, the temperature is taken as constant within a disc corresponding to the region illuminated by the laser beam of radius r_0; outside this region, the temperature drops as $1/r$ along the radial coordinate r because of the conservation of heat flow in our disc geometry (Section 5 of Supporting Information). This contrasts with the constant temperature profile along ballistic conductors with uniform width. In the diffusive regime, the temperature decreases logarithmically along r due to phonon scattering events.[56,82,83] The measured C and K are converted into c and κ using

$$c = \frac{C}{\pi R_0^2 t \rho}\beta \tag{3}$$

$$\kappa = \frac{K}{2\pi t}\eta \tag{4}$$

where R_0 is the radius of the suspended drum, $t = 0.64$ nm the thickness of the monolayer, and ρ the mass density of $MoSe_2$. The geometrical constants β and η are of the order of one and depend on R_0, r_0, and the temperature profile (Section 5 of Supporting Information). The conductivity in Figure 4b is determined in the diffusive regime only.

The measured temperature dependence of κ above ∼100 K can be described by first-principles calculations on $MoSe_2$ monolayers in the diffusive regime (Figure 4b), whereas the measured temperature dependencies of c and K below ∼100 K are consistent with predictions in the ballistic regime (Figures 4b and 5d). For the comparison between measurements and theory, we derive the ballistic conductance in our peculiar disc geometry assuming that the inner reservoir is given by the radius r_0 and the outer reservoir by R_0. We obtain

$$K = 2\pi r_0 t \alpha \cdot \frac{\rho c v}{2} \tag{5}$$

$$v = \frac{\sum_{q,s} C_{q,s} \frac{2|v_{q,s}|}{\pi}}{\sum_{q,s} C_{q,s}} \tag{6}$$

where $C_{q,s} = \frac{dn_{q,s}}{dT}\hbar\omega_{q,s}$ is the specific heat of the phonon of the branch s with momenta q, $\omega_{q,s}$ is the phonon pulsation, $n_{q,s}$ is the Bose occupation factor, and $v_{q,s}$ is the group velocity. The constant α is another geometric factor of the order of one like β and η. The expression of these three geometrical factors is given in eqs S34, S50, and after S26 of Supporting Information. The phonon properties of the monolayer lattice are calculated using density functional perturbation theory. Instead, in the diffusive regime the conductivity is derived by an exact solution of the Boltzmann transport equation taking into account three-phonon interactions and isotopic scattering.[84] In such a calculation, we use scattering rates derived by first-principles that depend on the energy and momentum of the involved phonons, in contrast to the single empirical effective time τ used in eqs 1 and 2, which describes the characteristic time for the heat to travel out of the resonator. The conductivity derived with a homogeneous temperature gradient (∇T) can be compared to the measured conductance through eq 4, which maps transport with nonhomogenous ∇T to that with homogeneous ∇T. The derivation of eqs 3−6 and information on the first-principle calculations can be found in Section 5 of Supporting Information. The reasonably good agreement between measurement and theory in Figure 4b suggests that the resistance at the interface between the monolayer and the substrate does not contribute significantly to the thermal transport. Future work will be carried out on smaller diameter drums where the resistance of the interface is expected to become comparatively larger.

Our optomechanical measurements provide a detailed picture of thermal transport in monolayer $MoSe_2$ lattices down to cryogenic temperature. Our work opens the possibility to measure thermal properties in a large variety of different two-dimensional materials, because the devices required for these measurements are simple to fabricate. We will improve the quality factor of drums by, for example, increasing their diameter in order to measure τ and the heat capacity up to room temperature. This new measurement method may allow the exploration of the phonon hydro-

DOI: 10.1021/acs.nanolett.9b00560
Nano Lett. 2019, 19, 3143−3150

dynamics regime, which is expected to be robust in monolayer systems.[66,67] This regime is interesting because heat is carried by collective excitations of phonon states. This gives rise to a new type of sound propagation, called second sound. The measurement of τ should enable the direct access of the velocity of the second sound. In addition, this new measurement method may shed light on the divergence of the thermal conductivity in two-dimensions, when the size of the system increases.[50] The origin of this behavior is under active investigation with different interpretations based on either the dimensionality of the system or the special phononic states that remain ballistic over extraordinarily long distances.[79,85,86] Optomechanical measurements also enable the study of the anisotropic thermal conductivity, as recently demonstrated in 10−100 nm thick black phosphorus crystals at room temperature.[87]

■ ASSOCIATED CONTENT

Supporting Information

The Supporting Information is available free of charge on the ACS Publications website at DOI: 10.1021/acs.nanolett.9b00560.

Further information on the characterization of monolayers, the absorption of suspended monolayers, the mechanical tension of membranes, the measurements of the equivalent thermal conductance and the heat capacity, and the predictions based on first-principles (PDF)

■ AUTHOR INFORMATION

Corresponding Author

*E-mail: adrian.bachtold@icfo.eu

ORCID

Adrian Bachtold: 0000-0002-6145-2479

Author Contributions

N.M. fabricated the devices. N.M., S.T., and A.R.P. carried out the experiment with support from M.M. and X.M. A.C. did the first-principles calculations. A.C. and F.M. developed the model of the thermal transport in the ballistic regime with contributions from A.I. and A.B. I.E. carried out the simulations of the interference pattern of the laser beam. The data analysis was done by N.M. and A.B. N.M. and A.B. wrote the manuscript with comments from the other authors. A.B. supervised the work.

Notes

The authors declare no competing financial interest.

■ ACKNOWLEDGMENTS

This work is supported by the ERC advanced Grant 692876, the Foundation Cellex, the CERCA Programme, AGAUR, Severo Ochoa (SEV-2015-0522), the Grant FIS2015-69831-P of MINECO, the Fondo Europeo de Desarrollo Regional (FEDER), and the Project P2ELP2-168546 of the Swiss National Science Foundation.

■ REFERENCES

(1) Lee, J.; Wang, Z.; He, K.; Shan, J.; Feng, P. X. L. High frequency MoS_2 nanomechanical resonators. *ACS Nano* **2013**, *7*, 6086−6091.

(2) Castellanos-Gomez, A.; van Leeuwen, R.; Buscema, M.; van der Zant, H. S.; Steele, G. A.; Venstra, W. J. Single-Layer MoS_2 Mechanical Resonators. *Adv. Mater.* **2013**, *25*, 6719−6723.

(3) Morell, N.; Reserbat-Plantey, A.; Tsioutsios, I.; Schaedler, K. G.; Dubin, F.; Koppens, F. H.; Bachtold, A. High quality factor mechanical resonators based on WSe2 monolayers. *Nano Lett.* **2016**, *16*, 5102−5108.

(4) Lee, J.; Wang, Z.; He, K.; Yang, R.; Shan, J.; Feng, X. L. Electrically tunable single- and few-layer MoS2 nanoelectromechanical systems with broad dynamic range. *Science Adv.* **2018**, *4*, No. eaao6653.

(5) Bunch, J. S.; van der Zande, A. M.; Verbridge, S. S.; Frank, I. W.; Tanenbaum, D. M.; Parpia, J. M.; Craighead, H. G.; McEuen, P. L. Electromechanical resonators from graphene sheets. *Science* **2007**, *315*, 490−493.

(6) Chen, C.; Rosenblatt, S.; Bolotin, K.; Kalb, W.; Kim, P.; Kymissis, I.; Stormer, H.; Heinz, T.; Hone, J. Performance of monolayer graphene nanomechanical resonators with electrical readout. *Nat. Nanotechnol.* **2009**, *4* (12), 861.

(7) Eichler, A.; Moser, J.; Chaste, J.; Zdrojek, M.; Wilson-Rae, I.; Bachtold, A. Nonlinear damping in mechanical resonators made from carbon nanotubes and graphene. *Nat. Nanotechnol.* **2011**, *6*, 339−342.

(8) Miao, T.; Yeom, S.; Wang, P.; Standley, B.; Bockrath, M. Graphene nanoelectromechanical systems as stochastic-frequency oscillators. *Nano Lett.* **2014**, *14*, 2982.

(9) Singh, V.; Bosman, S. J.; Schneider, B. H.; Blanter, Y. M.; Castellanos-Gomez, A.; Steele, G. A. Optomechanical coupling between a graphene mechanical resonator and a superconducting microwave cavity. *Nat. Nanotechnol.* **2014**, *9*, 820−824.

(10) Song, X.; Oksanen, M.; Li, J.; Hakonen, P. J.; Sillanpää, M. A. Graphene optomechanics realized at microwave frequencies. *Phys. Rev. Lett.* **2014**, *113*, 027404.

(11) Weber, P.; Güttinger, J.; Tsioutsios, I.; Chang, D. E.; Bachtold, A. Coupling graphene mechanical resonators to superconducting microwave cavities. *Nano Lett.* **2014**, *14* (5), 2854−60.

(12) Cole, R. M.; Brawley, G. A.; Adiga, V. P.; De Alba, R.; Parpia, J. M.; Ilic, B.; Craighead, H. G.; Bowen, W. P. Evanescent-Field Optical Readout of Graphene Mechanical Motion at Room Temperature. *Phys. Rev. Appl.* **2015**, *3*, 024004.

(13) De Alba, R.; Massel, F.; Storch, I. R.; Abhilash, T. S.; Hui, A.; McEuen, P. L.; Craighead, H. G.; Parpia, J. M. Tunable phonon-cavity coupling in graphene membranes. *Nat. Nanotechnol.* **2016**, *11*, 741−746.

(14) Mathew, J. P.; Patel, R. N.; Borah, A.; Vijay, R.; Deshmukh, M. M. Dynamical strong coupling and parametric amplification of mechanical modes of graphene drums. *Nat. Nanotechnol.* **2016**, *11*, 747−751.

(15) Guttinger, J.; Noury, A.; Weber, P.; Eriksson, A. M.; Lagoin, L.; Moser, J.; Eichler, C.; Wallraff, A.; Isacsson, A.; Bachtold, A. Energy-dependent path of dissipation in nanomechanical resonators. *Nat. Nanotechnol.* **2017**, *12*, 631.

(16) Will, M.; Hamer, M.; Müller, M.; Noury, A.; Weber, P.; Bachtold, A.; Gorbachev, R. V.; Stampfer, C.; Guttinger, J. High Quality Factor Graphene-Based Two-Dimensional Heterostructure Mechanical Resonator. *Nano Lett.* **2017**, *17*, 5950−5955.

(17) Sazonova, V.; Yaish, Y.; Ustunel, H.; Roundy, D.; Arias, T. A.; McEuen, P. L. A tunable carbon nanotube electromechanical oscillator. *Nature* **2004**, *431*, 284−287.

(18) Lassagne, B.; Tarakanov, Y.; Kinaret, J.; Garcia-Sanchez, D.; Bachtold, A. Coupling mechanics to charge transport in carbon nanotube mechanical resonators. *Science* **2009**, *325*, 1107−1110.

(19) Steele, G. A.; Hüttel, A. K.; Witkamp, B.; Poot, M.; Meerwaldt, H. B.; Kouwenhoven, L. P.; van der Zant, H. S. J. Strong coupling between single-electron tunneling and nanomechanical motion. *Science* **2009**, *325*, 1103−1107.

(20) Gouttenoire, V.; Barois, T.; Perisanu, S.; Leclercq, J.-L.; Purcell, S. T.; Vincent, P.; Ayari, A. Digital and FM demodulation of a doubly clamped single-walled carbon-nanotube oscillator: towards a nanotube cell phone. *Small* **2010**, *6*, 1060−1065.

(21) Chaste, J.; Eichler, A.; Moser, J.; Ceballos, G.; Rurali, R.; Bachtold, A. A nanomechanical mass sensor with yoctogram resolution. *Nat. Nanotechnol.* **2012**, *7*, 301−304.

DOI: 10.1021/acs.nanolett.9b00560
Nano Lett. 2019, 19, 3143−3150

(22) Stapfner, S.; Ost, L.; Hunger, D.; Reichel, J.; Favero, I.; Weig, E. M. Cavity-enhanced optical detection of carbon nanotube Brownian motion. *Appl. Phys. Lett.* **2013**, *102*, 151910.
(23) Moser, J.; Güttinger, J.; Eichler, A.; Esplandiu, M. J.; Liu, D. E.; Dykman, M. I.; Bachtold, A. Ultrasensitive force detection with a nanotube mechanical resonator. *Nat. Nanotechnol.* **2013**, *8*, 493−496.
(24) Ganzhorn, M.; Wernsdorfer, W. Dynamics and dissipation induced by single-electron tunneling in carbon nanotube nano-electromechanical systems. *Phys. Rev. Lett.* **2012**, *108*, 175502.
(25) Benyamini, A.; Hamo, A.; Kusminskiy, S. V.; von Oppen, F.; Ilani, S. Real-space tailoring of the electron−phonon coupling in ultraclean nanotube mechanical resonators. *Nat. Phys.* **2014**, *10*, 151−156.
(26) Tavernarakis, A.; Stavrinadis, A.; Nowak, A.; Tsioutsios, I.; Bachtold, A.; Verlot, P. Optomechanics with a hybrid carbon nanotube resonator. *Nat. Commun.* **2018**, *9*, 662.
(27) de Bonis, S. L.; Urgell, C.; Yang, W.; Samanta, C.; Noury, A.; Vergara-Cruz, J.; Dong, Q.; Jin, Y.; Bachtold, A. Ultrasensitive Displacement Noise Measurement of Carbon Nanotube Mechanical Resonators. *Nano Lett.* **2018**, *18*, 5324.
(28) Khivrich, I.; Clerk, A. A.; Ilani, S. Nanomechanical pump-probe measurements of insulating electronic states in a carbon nanotube. *Nat. Nanotechnol.* **2019**, *14*, 161.
(29) Ayari, A.; Vincent, P.; Perisanu, S.; Choueib, M.; Gouttenoire, V.; Bechelany, M.; Cornu, D.; Purcell, S. T. Self-oscillations in field emission nanowire mechanical resonators: A nanometric dc-ac conversion. *Nano Lett.* **2007**, *7* (8), 2252−2257.
(30) Gil-Santos, E.; Ramos, D.; Martinez, J.; Fernandez-Regulez, M.; Garcia, R.; San Paulo, A.; Calleja, M.; Tamayo, J. Nanomechanical mass sensing and stiffness spectrometry based on two-dimensional vibrations of resonant nanowires. *Nat. Nanotechnol.* **2010**, *5* (9), 641−645.
(31) Nichol, J. M.; Naibert, T. R.; Hemesath, E. R.; Lauhon, L. J.; Budakian, R. Nanoscale Fourier-transform magnetic resonance imaging. *Phys. Rev. X* **2013**, *3*, 031016.
(32) Gloppe, A.; Verlot, P.; Dupont-Ferrier, E.; Siria, A.; Poncharal, P.; Bachelier, G.; Vincent, P.; Arcizet, O.; Dupont-Ferrier, E.; Siria, A.; Poncharal, P.; Bachelier, G.; Vincent, P.; Arcizet, O. Bidimensional nano-optomechanics and topological backaction in a non-conservative radiation force field. *Nat. Nanotechnol.* **2014**, *9* (11), 920−926.
(33) Nigués, A.; Siria, A.; Verlot, P. Dynamical Backaction Cooling with Free Electrons. *Nat. Commun.* **2015**, *6*, 8014.
(34) Sansa, M.; Fernandez-Regulez, M.; Llobet, L.; San Paulo, A.; Perez-Murano, F. High-sensitivity linear piezoresistive transduction for nanomechanical beam resonators. *Nat. Commun.* **2014**, *5*, 4313.
(35) Rossi, N.; Braakman, F. R.; Cadeddu, D.; Vasyukov, D.; Tütüncüoglu, G.; Fontcuberta i Morral, A.; Poggio, M. Vectorial scanning force microscopy using a nanowire sensor. *Nat. Nanotechnol.* **2016**, *12*, 150−155.
(36) Mercier de Lépinay, L.; Pigeau, B.; Besga, B.; Vincent, P.; Poncharal, P.; Arcizet, O. Universal Vectorial and Ultrasensitive Nanomechanical Force Field Sensor. *Nat. Nanotechnol.* **2016**, *12*, 156−162.
(37) Hanay, M. S.; Kelber, S.; Naik, A. K.; Chi, D.; Hentz, S.; Bullard, E. C.; Colinet, E.; Duraffourg, L.; Roukes, M. L. Single-protein nanomechanical mass spectrometry in real time. *Nat. Nanotechnol.* **2012**, *7*, 602−608.
(38) Losby, J. E.; Sani, F. F.; Grandmont, D. T.; Diao, Z.; Belov, M.; Burgess, J. A. J.; Compton, S. R.; Hiebert, W. K.; Vick, D.; Mohammad, K.; Salimi, E.; Bridges, G. E.; Thomson, D. J.; Freeman, M. R. Torque-mixing magnetic resonance spectroscopy. *Science* **2015**, *350*, 798−801.
(39) Mehlin, A.; Xue, F.; Liang, D.; Du, H. F.; Stolt, M. J.; Jin, S.; Tian, M. L.; Poggio, M. Stabilized skyrmion phase detected in MnSi nanowires by dynamic cantilever magnetometry. *Nano Lett.* **2015**, *15* (7), 4839−4844.
(40) Wang, Z.; Wei, J.; Morse, P.; Dash, J. G.; Vilches, O. E.; Cobden, D. H. Phase transitions of adsorbed atoms on the surface of a carbon nanotube. *Science* **2010**, *327*, 552−555.
(41) Tavernarakis, A.; Chaste, J.; Eichler, A.; Ceballos, G.; Gordillo, M. C.; Boronat, J.; Bachtold, A. Atomic monolayer deposition on the surface of nanotube mechanical resonators. *Phys. Rev. Lett.* **2014**, *112*, 196103.
(42) Bleszynski-Jayich, A. C.; Shanks, W. E.; Peaudecerf, B.; Ginossar, E.; von Oppen, F.; Glazman, L.; Harris, J. G. E. *Science* **2009**, *326*, 272.
(43) Schwab, K.; Henriksen, E. A.; Worlock, J. M.; Roukes, M. L. Measurement of the quantum of thermal conductance. *Nature* **2000**, *404*, 974.
(44) Li, N.; Ren, J.; Wang, L.; Zhang, G.; Hänggi, P.; Li, B. Colloquium: Phononics: Manipulating heat flow with electronic analogs and beyond. *Rev. Mod. Phys.* **2012**, *84*, 1045.
(45) Tavakoli, A.; Lulla, K.; Crozes, T.; Mingo, N.; Collin, E.; Bourgeois, O. Heat conduction measurements in ballistic 1D phonon waveguides indicate breakdown of the thermal conductance quantization. *Nat. Commun.* **2018**, *9* (1), 4287.
(46) Bauer, G. E.; Saitoh, E.; Van Wees, B. J. Spin caloritronics. *Nat. Mater.* **2012**, *11*, 391−399.
(47) Giazotto, F.; Heikkilä, T. T.; Luukanen, A.; Savin, A. M.; Pekola, J. P. Opportunities for mesoscopics in thermometry and refrigeration: Physics and applications. *Rev. Mod. Phys.* **2006**, *78*, 217.
(48) Jezouin, S.; Parmentier, F. D.; Anthore, A.; Gennser, U.; Cavanna, A.; Jin, Y.; Pierre, F. Quantum limit of heat flow across a single electronic channel. *Science* **2013**, *342* (6158), 601−604.
(49) Pekola, J. P. Towards quantum thermodynamics in electronic circuits. *Nat. Phys.* **2015**, *11*, 118−123.
(50) Xu, X.; Pereira, L. F.; Wang, Y.; Wu, J.; Zhang, K.; Zhao, X.; Bae, S.; Bui, C. T.; Xie, R.; Thong, J. T.; Hong, B. H.; et al. Length-dependent thermal conductivity in suspended single-layer graphene. *Nat. Commun.* **2014**, *5*, 3689.
(51) Kim, P.; Shi, L.; Majumdar, A.; McEuen, P. L. Thermal transport measurements of individual multiwalled nanotubes. *Phys. Rev. Lett.* **2001**, *87*, 215502.
(52) Yu, C.; Shi, L.; Yao, Z.; Li, D.; Majumdar, A. Thermal conductance and thermopower of an individual single-wall carbon nanotube. *Nano Lett.* **2005**, *5*, 1842−1846.
(53) Balandin, A. A. Thermal properties of graphene and nanostructured carbon materials. *Nat. Mater.* **2011**, *10*, 569−581.
(54) Yan, R.; Simpson, J. R.; Bertolazzi, S.; Brivio, J.; Watson, M.; Wu, X.; Kis, A.; Luo, T.; Hight Walker, A. R.; Xing, H. G. Thermal conductivity of monolayer molybdenum disulfide obtained from temperature-dependent Raman spectroscopy. *ACS Nano* **2014**, *8*, 986−993.
(55) Balandin, A. A.; Ghosh, S.; Bao, W.; Calizo, I.; Teweldebrhan, D.; Miao, F.; Lau, C. N. Superior thermal conductivity of single-layer graphene. *Nano Lett.* **2008**, *8*, 902−907.
(56) Cai, W.; Moore, A. L.; Zhu, Y.; Li, X.; Chen, S.; Shi, L.; Ruoff, R. S. Thermal transport in suspended and supported monolayer graphene grown by chemical vapor deposition. *Nano Lett.* **2010**, *10*, 1645−1651.
(57) Ghosh, S.; Bao, W.; Nika, D. L.; Subrina, S.; Pokatilov, E. P.; Lau, C. N.; Balandin, A. A. Dimensional crossover of thermal transport in few-layer graphene. *Nat. Mater.* **2010**, *9*, 555−558.
(58) Faugeras, C.; Faugeras, B.; Orlita, M.; Potemski, M.; Nair, R. R.; Geim, A. K. Thermal conductivity of graphene in corbino membrane geometry. *ACS Nano* **2010**, *4*, 1889−1892.
(59) Lee, J. U.; Yoon, D.; Kim, H.; Lee, S. W.; Cheong, H. Thermal conductivity of suspended pristine graphene measured by Raman spectroscopy. *Phys. Rev. B: Condens. Matter Mater. Phys.* **2011**, *83*, 081419.
(60) Zhang, X.; Sun, D.; Li, Y.; Lee, G.-H.; Cui, X.; Chenet, D.; You, Y.; Heinz, T. F.; Hone, J. C. Measurement of Lateral and Interfacial Thermal Conductivity of Single- and Bilayer MoS2 and MoSe2 Using Refined Optothermal Raman Technique. *ACS Appl. Mater. Interfaces* **2015**, *7*, 25923.
(61) Sledzinska, M.; Graczykowski, B.; Placidi, M.; Reig, D. S.; Sachat, A. E.; Reparaz, J. S.; Alzina, F.; Mortazavi, B.; Quey, R.; Colombo, L.; Roche, S.; Sotomayor, C. M. Record Low Thermal

DOI: 10.1021/acs.nanolett.9b00560
Nano Lett. 2019, 19, 3143−3150

Conductivity of Polycrystalline MoS2 Films: Tuning the Thermal Conductivity by Grain Orientation. *2D Mater.* **2016**, *3*, 035016.
(62) Ye, F.; Lee, J.; Feng, P. X. L. Electrothermally Tunable Graphene Resonators Operating at Very High Temperature up to 1200 K. *Nano Lett.* **2018**, *18*, 1678−1685.
(63) Shi, L.; Zhou, J.; Kim, P.; Bachtold, A.; Majumdar, A.; McEuen, P. L. Thermal probing of energy dissipation in current-carrying carbon nanotubes. *J. Appl. Phys.* **2009**, *105* (10), 104306.
(64) Pumarol, M. E.; Rosamond, M. C.; Tovee, P.; Petty, M. C.; Zeze, D. A.; Falko, V.; Kolosov, O. V. Direct nanoscale imaging of ballistic and diffusive thermal transport in graphene nanostructures. *Nano Lett.* **2012**, *12* (6), 2906−2911.
(65) Bae, M. H.; Li, Z.; Aksamija, Z.; Martin, P. N.; Xiong, F.; Ong, Z. Y.; Knezevic, I.; Pop, E. Ballistic to diffusive crossover of heat flow in graphene ribbons. *Nat. Commun.* **2013**, *4*, 1734.
(66) Cepellotti, A.; Fugallo, G.; Paulatto, L.; Lazzeri, M.; Mauri, F.; Marzari, N. Phonon hydrodynamics in two-dimensional materials. *Nat. Commun.* **2015**, *6*, 6400.
(67) Lee, S.; Broido, D.; Esfarjani, K.; Chen, G. Hydrodynamic phonon transport in suspended graphene. *Nat. Commun.* **2015**, *6*, 6290.
(68) Crossno, J.; Shi, J. K.; Wang, K.; Liu, X.; Harzheim, A.; Lucas, A.; Sachdev, S.; Kim, P.; Taniguchi, T.; Watanabe, K.; Ohki, T. A.; Fong, K. C. Observation of the Dirac fluid and the breakdown of the Wiedemann-Franz law in graphene. *Science* **2016**, *351*, 1058.
(69) Efetov, D. K.; Shiue, R. J.; Gao, Y.; Skinner, B.; Walsh, E. D.; Choi, H.; Zheng, J.; Tan, C.; Grosso, G.; Peng, C.; Hone, J.; Fong, K. C.; Englund, D. Fast thermal relaxation in cavity-coupled graphene bolometers with a Johnson noise read-out. *Nat. Nanotechnol.* **2018**, *13*, 797−801.
(70) Metzger, C.; Favero, I.; Ortlieb, A.; Karrai, K. Optical self cooling of a deformable Fabry-Perot cavity in the classical limit. *Phys. Rev. B: Condens. Matter Mater. Phys.* **2008**, *78*, 035309.
(71) Schwarz, C. Optomechanical, vibrational and thermal properties of suspended graphene membranes. Ph.D. Thesis, University Grenoble Alpes, Grenoble, France, 2016.
(72) Dolleman, R. J.; Houri, S.; Davidovikj, D.; Cartamil-Bueno, S. J.; Blanter, Y. M.; van der Zant, H. S.; Steeneken, P. G. Optomechanics for thermal characterization of suspended graphene. *Phys. Rev. B: Condens. Matter Mater. Phys.* **2017**, *96* (16), 165421.
(73) Metzger, C. H.; Karrai, K. Cavity cooling of a microlever. *Nature* **2004**, *432*, 1002−1005.
(74) Barton, R. A.; Storch, I. R.; Adiga, V. P.; Sakakibara, R.; Cipriany, B. R.; Ilic, B.; Wang, S. P.; Ong, P.; McEuen, P. L.; Parpia, J. M.; Craighead, H. G. Photothermal self-oscillation and laser cooling of graphene optomechanical systems. *Nano Lett.* **2012**, *12*, 4681−4686.
(75) Castellanos-Gomez, A.; Buscema, M.; Molenaar, R.; Singh, V.; Janssen, L.; van der Zant, H. S. J.; Steele, G. A. Deterministic transfer of two-dimensional materials by all-dry viscoelastic stamping. *2D Mater.* **2014**, *1*, 011002.
(76) Ross, J. S.; Wu, S.; Yu, H.; Ghimire, N. J.; Jones, A. M.; Aivazian, G.; Yan, J.; Mandrus, D. G.; Xiao, D.; Yao, W.; Xu, X. Electrical control of neutral and charged excitons in a monolayer semiconductor. *Nat. Commun.* **2013**, *4*, 1474.
(77) Wang, G.; Palleau, E.; Amand, T.; Tongay, S.; Marie, X.; Urbaszek, B. Polarization and time-resolved photoluminescence spectroscopy of excitons in MoSe2 monolayers. *Appl. Phys. Lett.* **2015**, *106* (11), 112101.
(78) Taube, A.; Judek, J.; Lapinska, A.; Zdrojek, M. Temperature-dependent thermal properties of supported MoS_2 monolayers. *ACS Appl. Mater. Interfaces* **2015**, *7*, 5061.
(79) Fugallo, G.; Cepellotti, A.; Paulatto, L.; Lazzeri, M.; Marzari, N.; Mauri, F. Thermal conductivity of graphene and graphite: collective excitations and mean free paths. *Nano Lett.* **2014**, *14*, 6109−6114.
(80) Hone, J.; Batlogg, B.; Benes, Z.; Johnson, A. T.; Fischer, J. E. Quantized phonon spectrum of single-wall carbon nanotubes. *Science* **2000**, *289*, 1730−1733.
(81) Kiwia, H. L.; Westrum, E. F., Jr Low-temperature heat capacities of molybdenum diselenide and ditelluride. *J. Chem. Thermodyn.* **1975**, *7*, 683−691.
(82) Johnson, J. A.; Maznev, A. A.; Cuffe, J.; Eliason, J. K.; Minnich, A. J.; Kehoe, T.; Sotomayor Torres, C. M.; Chen, G.; Nelson, K. A. Direct measurement of room-temperature nondiffusive thermal transport over micron distances in a silicon membrane. *Phys. Rev. Lett.* **2013**, *110*, 025901.
(83) Cepellotti, A.; Marzari. N Boltzmann transport in nanostructures as a friction effect. *Nano Lett.* **2017**, *17*, 4675.
(84) Fugallo, G.; Lazzeri, M.; Paulatto, L.; Mauri, F. Ab initio variational approach for evaluating lattice thermal conductivity. *Phys. Rev. B: Condens. Matter Mater. Phys.* **2013**, *88*, 045430.
(85) Lepri, S.; Livi, R.; Politi, A. Thermal conduction in classical low-dimensional lattices. *Phys. Rep.* **2003**, *377*, 1−80.
(86) Lindsay, L.; Li, W.; Carrete, J.; Mingo, N.; Broido, D. A.; Reinecke, T. L. Phonon thermal transport in strained and unstrained graphene from first principles. *Phys. Rev. B: Condens. Matter Mater. Phys.* **2014**, *89*, 155426.
(87) Islam, A.; van den Akker, A.; Feng, P. X.-L. Anisotropic thermal conductivity of suspended black phosphorus probed by opto-thermomechanical resonance spectromicroscopy. *Nano Lett.* **2018**, *18*, 7683.

DOI: 10.1021/acs.nanolett.9b00560
Nano Lett. 2019, 19, 3143−3150